Non-Proliferative Diabetic Retinopathy Is Characterized by Nonuniform Alterations of Peripapillary Capillary Networks

Dong An,[1] Erandi Chandrasekera,[1] Dao-Yi Yu,[1,2] and Chandrakumar Balaratnasingam[1–3]

[1]Centre for Ophthalmology and Visual Science, University of Western Australia, Perth, Australia
[2]Lions Eye Institute, Nedlands, Western Australia, Australia
[3]Department of Ophthalmology, Sir Charles Gairdner Hospital, Western Australia, Australia

Correspondence: Dao-Yi Yu, Centre for Ophthalmology and Visual Science, The University of Western Australia, Nedlands, Western Australia, 6009, Australia; dyyu@lei.org.au.

DA and EC contributed equally to the work presented here and should, therefore, be regarded as equivalent first authors.

Received: April 12, 2019
Accepted: February 9, 2020
Published: April 27, 2020

Citation: An D, Chandrasekera E, Yu D-Y, Balaratnasingam C. Non-proliferative diabetic retinopathy is characterized by nonuniform alterations of peripapillary capillary networks. *Invest Ophthalmol Vis Sci.* 2020;61(4):39. https://doi.org/10.1167/iovs.61.4.39

Purpose. The purpose of this study was to use three-dimensional confocal microscopy to quantify the spatial patterns of capillary network alterations in nonproliferative diabetic retinopathy (NPDR).

Methods. The retinal microvasculature was perfusion-labelled in seven normal human donor eyes and six age-matched donor eyes with NPDR. The peripapillary microcirculation was studied using confocal scanning laser microscopy. Capillary density and diameters of the radial peripapillary capillary plexus (RPCP), superficial capillary plexus (SCP), intermediate capillary plexus (ICP), and deep capillary plexus (DCP) were quantified and compared. Three-dimensional visualization strategies were also used to compare the communications between capillary beds and precapillary arterioles and postcapillary venules.

Results. Mean capillary diameter was significantly increased in the NPDR group ($P < 0.001$). Intercapillary distance was significantly increased in the DCP ($P = 0.004$) and RPCP ($P = 0.022$) of the NPDR group ($P = 0.010$) but not the SCP ($P = 0.155$) or ICP ($P = 0.103$). The NPDR group was associated with an increased frequency of inflow communication between the SCP and ICP/DCP and a decreased frequency of communication between the SCP and RPCP ($P = 0.023$). There was no difference in the patterns of outflow communications between the two groups ($P = 0.771$).

Conclusions. This study demonstrates that capillary plexuses are nonuniformly perturbed in NPDR. These structural changes may be indicative of perturbations to blood flow patterns between different retinal layers. Our findings may aid the interpretation of previous clinical observations made using optical coherence tomography angiography as well as improve our understanding of the pathogenesis of NPDR.

Keywords: diabetes, retina, capillary, microcirculation, optic disc, vascular disease

Microvascular alterations are the hallmark feature of diabetic retinopathy (DR); a major cause of visual morbidity worldwide.[1,2] Detailed histologic studies have defined the ultrastructural changes that characterize DR, such as microaneurysms, intraretinal vascular anomalies, capillary closure, cotton-wool spots, and retinal oedema.[1,3–7] The cellular disturbances that underlie each of the ultrastructural manifestations, including pericyte loss,[1,8] basement membrane degeneration,[9] endothelial proliferation,[10] and endothelial apoptosis[11] have also been defined in experimental and postmortem examinations. Collectively, these studies have delineated the sequence of neural, glia, and vascular alterations during the progressive stages of DR and have provided valuable insights into the pathogenesis of this disease. What is less clearly understood is the spatial profile of microvascular alterations due to DR and whether all capillary networks within a defined volume of retinal tissue are affected equally. This is a fundamental question that has major relevance for improving our understanding of the pathogenesis and natural history of DR.

The retinal circulation is a critical source of energy substrates for neurons and is morphologically specialized with respect to retinal eccentricity and the retinal layer traversed by the capillary vascular system.[12–16] The unique energy demands of retinal layers coupled with regional variations in angio-architectural characteristics make it likely that certain retinal layers are more, or less, vulnerable to metabolic injury. Although clinical imaging studies have indicated that the deep vascular beds of the retina are relatively more susceptible to structural alterations in DR,[17–21] this has not been clearly highlighted using histologic techniques. An important reason for this gap in knowledge is the widespread use of tissue digestion techniques in previous histologic reports, making it difficult to precisely delineate vascular changes relative to retinal depth. Clarifying this issue is likely to improve our understanding of DR pathophysiology.

Copyright 2020 The Authors

This work is licensed under a Creative Commons Attribution-NonCommercial-NoDerivatives 4.0 International License.

Table 1. Demographic and Clinical Details of Human Donor Eyes

Donor	Side	Group	Cause of Death	Sex	Age, y	HTN	Time to Cannulation, h
1	L	D	Myocardial infarction	M	66	Y	21
2	L	D	Right subarachnoid hemorrhage	M	85	Y	1
3	R & L	D	Myocardial infarction	M	84	N	9
4	R & L	D	Myocardial infarction	F	52	N	5
5	R	D	Bowel cancer	F	60	N	3
6	R & L	C	Cancer	F	75	Y	4
7	L	C	Sepsis	F	74	N	3
8	R	C	Cancer	F	67	N	9
9	R & L	C	Ischemic stroke	F	89	Y	4

C, control; D, diabetes; F, female; M, male; L, left; R, right; HTN, hypertension; Y, Yes; N, No.

The principle aim of this study is to determine if the capillary plexuses of the human retinal circulation are uniformly perturbed in the nonproliferative stages of DR (NPDR). In this report, we perform a detailed quantitative analysis involving capillary diameter and intercapillary distance[22–25] of the peripapillary capillary plexuses using two-dimensional and three-dimensional histologic imaging techniques. Perfusion-labeled human donor eyes from patients that manifest NPDR are used. The results of this study expand our understanding of the pathobiology of DR and also assist in the clinical application of vascular imaging techniques, such as optical coherence tomography angiography (OCTA), to better detect and quantify retinal changes due to DR. It is also an important extension of previous studies that have used OCTA,[17,21,26,27] adaptive optics[28,29] and video fluorescein angiography[30,31] to define the patterns of capillary changes due to diabetic retinopathy.

Materials and Methods

The study was approved by the human research ethics committee at the University of Western Australia. All human tissue was handled according to the Tenets of the Declaration of Helsinki.

Donor Eyes

Human donor eyes used in this report were obtained from DonateLife WA (Perth, Western Australia), the organ and tissue retrieval authority in Western Australia, Australia. The demographic details, cause of death, and postmortem time to cannulation are presented in Table 1.

The donor cohort in this study was stratified into a control group and diabetes group. The control group comprised of eyes with no history of eye disease and no history of diabetes mellitus. The quantitative properties of the peripapillary circulation of eyes in the control group have been reported in our previous publication.[32] The diabetes group comprised of eyes from donors that upon medical record review were confirmed to have a diagnosis of type 2 diabetes mellitus. Only those eyes that demonstrated the histologic vascular alterations that characterize DR, such as microaneurysms, capillary nonperfusion, hemorrhages, and intraretinal microvascular abnormalities, were included in this study. Eyes from donors with diabetes mellitus that did not demonstrate the vascular alterations characteristic of DR on postmortem microscopic examination were not included in the study. Additionally, tissue that was deemed to be of poor quality such that it was not possible to perform reliable quantitative histologic analysis was excluded from this study.

Tissue Preparation

Eyes were enucleated shortly upon death. Enucleated eyes were transported in Ringers lactate solution that had been bubbled with a mixture of 5% CO_2/95% O_2. At the laboratory, the eye was placed in a custom-built eye holder and the portion of the central retinal artery, before it traversed the optic nerve sheath inferiorly, was identified and dissected free of retro-orbital fat under the operating microscope. Our method of micro-cannulation and targeted perfusion based labeling techniques was then utilized to label the vascular endothelium of the retinal microvasculature.[14,33] Eyes were cannulated using a glass micropipette (100 µm tip diameter), and subsequently perfused with 1% bovine serum albumin dissolved in Ringers lactate solution to wash out residual blood clots. Perfusion fixation was achieved with a solution of 4% paraformaldehyde for 20 minutes followed by 0.1 M phosphate buffer (PB) for 15 minutes. Eyes from all donors were perfused with 0.02 mg lectin-fluorescein isothiocyanate (FITC, Product No. L4895; Sigma-Aldrich, Darmstadt, Germany) in 0.4 mL PB by slow push over 30 seconds. After 12 minutes, the eye was perfused again with PB for 15 minutes to wash out excess labels. The perfusate for all eyes also contained 1 µg Hoechst (Product No. H6024; Sigma-Aldrich) for nuclear labeling.

Postperfusion, the eye was decannulated and dissected along the equator. The vitreous was carefully peeled and dissected from the retina. The posterior segment was then immersed in 4% paraformaldehyde for 12 hours. Next, the neuro-retina was detached from the retinal pigment epithelium. The optic nerve head was sectioned to be continuous with the retina. The retina was flat mounted on glass slide by making several radial incisions along the edge. Glycerol (MERCK Pty. Limited, Victoria, Australia) was added to enhance the optical quality of the tissue before placement of the coverslip.

Confocal Scanning Laser Microscopy

After cannulation and perfusion of the central retinal artery, all orders of the retinal microvasculature were examined to ensure complete perfusion and washout of blood from the retinal vasculature, as well as clear labeling of the endothelium and nuclei. Retina with embolic vascular occlusions and

Investigative Ophthalmology & Visual Science

retinas with excessive dye leakage, which prohibited reliable quantification of vessel density and diameter, were excluded from further analysis.

Images of the optic disk and peripapillary regions were captured using a confocal scanning laser microscope (Nikon Eclipse 90i; Nikon Corporation, Tokyo, Japan or Nikon Eclipse E800; Nikon Corporation, Tokyo, Japan). We evaluated the same regions as our previous report of control eyes.[32] Specifically, the superior, temporal, inferior, and nasal quadrants were imaged using a Nikon 10 × NA 0.45 dry objective lens, which gave a field of view of 1.27 mm × 1.27 mm. The axial resolution was 1.24 µm. Areas from all four quadrants in the peripapillary region were chosen to study capillary inflow and outflow patterns and were imaged with the Nikon 40 × NA 1.0 oil objective lens to ascertain greater detail. Using a motorized stage, a series of z-stacks were captured at the required location. Each z-stack consisted of a depth of optical sections, 1 µm apart, along the z-axis. The top and bottom of a stack were manually selected using the preview mode. The top of the stack was set when a vessel first appeared in the nerve fiber layer (NFL). The bottom of the stack was set to 20 µm beyond the last of the deep capillary plexus (DCP) vessel. Such a methodology ensured that all vessels within tissue volume were captured and that displaced capillaries in the outer retina due to macular edema were not excluded from image capture. Low-magnification images of the retina flat-mount were also acquired using a Nikon 4 × NA 0.2 dry objective lens and montaged together. Lectin-FITC labeling was visualized using 488 nm argon laser excitation with emissions detected through 515 nm band pass filters. Simultaneous scanning was done in each donor eye to visualize the nuclei using 408 nm argon laser excitation with emissions detected through a 450 nm band pass filter. All images in this paper were prepared using Adobe Photoshop CS4 (version 12.1; Adobe Systems Inc.) and Adobe Illustrator CS5 (version 15.1.0; Adobe Systems Inc.).

Image Analysis

Confocal image files were processed with IMARIS (Bitplane, Zurich, Switzerland) and/or ImageJ (Rasband, W.S., ImageJ, U. S. National Institutes of Health, Bethesda, MD).

The peripapillary circulation was stratified into the radial peripapillary capillary plexus (RPCP; at the level of the NFL), the superficial capillary plexus (SCP; at the level of the ganglion cell layer), the intermediate capillary plexus (ICP; at the inner border of the inner nuclear layer) and the DCP (at the boundary of the inner nuclear layer and outer plexiform layer [OPL]). Colocalization to nuclear label was used to stratify each plexus. Two-dimensional images (n = 224) were generated by projecting all confocal slices that comprised a single capillary plexus (using the 10 × lens) and were used to attain quantitative measurements. Measurements were acquired from the nasal, temporal, superior, and inferior parts of the peripapillary region. The following quantitative measurements were attained using our previously published criteria.[25,32]

1. Capillary diameter (Supplementary Fig. S1): defined as the perpendicular distance across the maximum chord axis of each vessel. Each two-dimensional image was partitioned into nine equal regions and measurements were obtained from each region to ensure representative sampling. Five capillaries were measured in each of the 9 regions resulting in 45 measurements per image and the average of these 45 measurements was used in the analysis. Only capillaries with clearly defined vessel lumens were measured. Capillaries that appeared to be occluded distally with limited vessel staining were avoided. Capillary segments adjacent to microaneurysms were also not measured in eyes in the diabetes group (Supplementary Fig. S1). All capillary diameters measured were luminal diameters, as lectin labels the luminal aspect of the vascular endothelium.[34]
2. Intercapillary distance was measured to estimate capillary density.[25,32] A 3 × 3 grid consisting of two equally spaced horizontal and two equally spaced vertical perpendicular line segments measuring 0.5 mm each were superimposed over images. The manual counts of capillary intersections across the four-line segments were recorded. For each two-dimensional image, the intercapillary distance was derived by dividing the total number of capillary intersections across the four-line segments by the total length covered by the four-line segments (2 mm).

Capillary diameter and density measurements were completed by two graders (D.A. and E.C.).

Three-dimensional images (n = 99), constructed using confocal volumes acquired with the Nikon 40 × NA 1.0 oil objective lens (field of view of 318.5 µm × 318.5 µm) were used to evaluate vascular branching patterns and connections between capillary beds, precapillary arterioles, and postcapillary venules. Three-dimensional images of each confocal stack were generated using the same methodology as described in our previous publication.[32] Using Imaris software, confocal volumes were rotated in the x, y, and z axes to precisely delineate the topologic characteristics of capillary plexuses and their connections to each other as well as feeding arterioles and draining venules. Inflow branching patterns of the SCP were categorized and the frequency of each branching pattern in the control and diabetes groups was determined. In order to ensure that the arterial side of the capillary circulation was evaluated, we examined the first branch point of the SCP. The four branching patterns were defined as per our previous publication as follows[32]:

- Type 1 branching pattern of the SCP: characterized by bifurcation of the superficial capillary segment such that one branch connected with the RPCP and the second branch remained in the plane of the SCP.
- Type 2 branching pattern of the SCP: characterized by bifurcation of the superficial capillary segment such that one branch connected with the ICP or DCP and the second branch remained in the plane of the SCP.
- Type 3 branching pattern of the SCP: characterized by bifurcation of the superficial capillary segment such that one branch connected with the RPCP and the second branch connected with the ICP or DCP.
- Type 4 branching pattern of the SCP: characterized by trifurcation of the superficial capillary segment such that one branch connected to the RPCP, a second branch connected with either the ICP or DCP, and a third branch that remained in the plane of the SCP.

Investigative Ophthalmology & Visual Science

Capillary outflow pathways were also categorized and the frequency of each branching pattern in the control and diabetes groups was determined, as per our previous publication.[32] In order to ensure that the venous side of the capillary circulation was evaluated, we examined the final branch point within the SCP prior to connecting to the draining venule. The four branching patterns were defined as follows:

- Type 1 outflow pattern: characterized by an RPC in the same plane of the SCP connecting with a single capillary segment of the SCP.
- Type 2 outflow pattern: characterized by a capillary of the ICP or DCP and a capillary in the same plane of the SCP connecting with a single capillary segment of the SCP.
- Type 3 outflow pattern: characterized by a capillary of the ICP or DCP and a capillary of the RPCP connecting with a single capillary segment of the SCP.
- Type 4 outflow pattern: characterized by a branch of the RPCP, a capillary of the ICP or DCP, and a capillary in the same plane of the SCP connecting with a single capillary segment of the SCP.

Statistical Analysis

Data were analyzed using R (a language and environment for statistical computing; R Foundation for Statistical Computing, Vienna, Austria. URL https://www.R-project.org/), SigmaPlot (version 12.0; SPSS, Chicago, IL) and SPSS Statistics for Windows (version 24.0; IBM Corp., Armonk, NY). Two multivariate linear mixed effects models were used to compare capillary diameter (CD) and intercapillary distance (ICD) measurements in the four capillary plexuses between the control and diabetes groups. The covariates modelled were age and time to cannulation. Sex was not used as a covariate due to uneven distribution of sex among the diabetes and control groups. The mixed effects used for comparison between control and DR eyes within a particular plexus was eye (left/right) nested in donor identity to account for intra-eye correlations, as well as intereye correlations in cases where both eyes from the same donor were quantified. For analyses involving all plexuses, the mixed effects used were layer nested in eye nested in donor identity. This accounted for correlations between each plexus in addition to the intra and intereye correlations. In any layer that was found to be significantly different, the four quadrants surrounding the optic disk were further analyzed to determine if any quadrants contributed significantly to the differences in that layer. A P value less than or equal to 0.050 was considered significant.

Chi-square tests were performed to determine whether there was any significant association in patterns of vascular branching between the control and diabetes groups. A chi-square test of independence was conducted between diabetes (two categories: diabetes and control) and arterial pattern (four categories: 1, 2, 3, and 4), as well as diabetes and venous pattern (four categories: 1, 2, 3, and 4). To follow up significant results, the residuals were analyzed to determine which patterns contributed to the association. Cells where the residual is greater than $\pm$ 2 were considered significant contributors.[35]

Results

General

The control group that was used for analysis comprised of six eyes from four female donors. The diabetes group that was used for analysis comprised of seven eyes from five donors (3 male and 2 female). One donor with no history of ocular or systemic disease and two donors with NPDR were perfusion labeled but excluded from the study due to poor quality images that precluded reliable quantification. None of the donors in the diabetes group demonstrated histologic features of proliferative diabetic retinopathy. There was no clinical record of review by an ophthalmologist for any of the donors and no past ocular history was noted in the medical records. Premortem clinical imaging data was not available for any of the donors and there was no evidence of laser photocoagulation in any of the donor retinas. Review of the medical records revealed that two donors in each group were previously diagnosed with systemic hypertension, which was managed with medical therapy. One donor in the diabetes group was a smoker of approximately 20 cigarettes per day.

The mean age of the control group was 76.2 $\pm$ 9.2 years (range, 67–89 years) and that of the diabetes group was 69.4 $\pm$ 7.8 years (range, 52–85 years). The difference in mean age was not significant between the two groups ($P = 0.219$). The mean death-to-enucleation time for the control group (5 $\pm$ 2.7 hours) and diabetes group (7.8 $\pm$ 7.9 hours) was not different ($P = 0.159$).

Ultrastructural Characteristics and Retinal Vascular Patterns in Control and Diabetes Groups

Retinas in the control group demonstrated complete filling of all orders of the retinal circulation, including arterioles, capillaries, and venules. A typical whole mount montage of a retina from the diabetes group is provided in Figure 1. Retinas in the diabetes group demonstrated a spectrum of vascular alterations, including capillary nonperfusion, venous beading, and microaneurysms (Fig. 1). All retinas in the DR group had severe NPDR.[36] These changes were most prominent in the posterior pole and peripheral retina. Staining of vessels and leakage of FITC-lectin was more frequently seen in eyes in the diabetes group compared to the control group.

Transverse histologic images of the peripapillary regions for control and diabetes groups are presented in Figure 2. In both groups, the peripapillary region was characterized by a layered microcirculation comprised of four capillary plexuses – RPCP, SCP, ICP, and DCP. Projection of confocal slices to produce a two-dimensional en face image demonstrated similarities in the morphology of each capillary plexus in the two groups (Fig. 3). Specifically, the RPCP was characterized by straight and long capillary segments that were oriented parallel to each other. The SCP was found in the plane of retinal arterioles and venules and was the only plexus to communicate directly with large order retinal vessels. We did not find any evidence of direct communication between retinal arterioles and venules with any of the other capillary plexuses in either group. Vessels of the ICP demonstrated a predominantly three-dimensional configuration, whereas the DCP was largely a planar vascular network characterized by multiple closed loops.

Investigative Ophthalmology & Visual Science

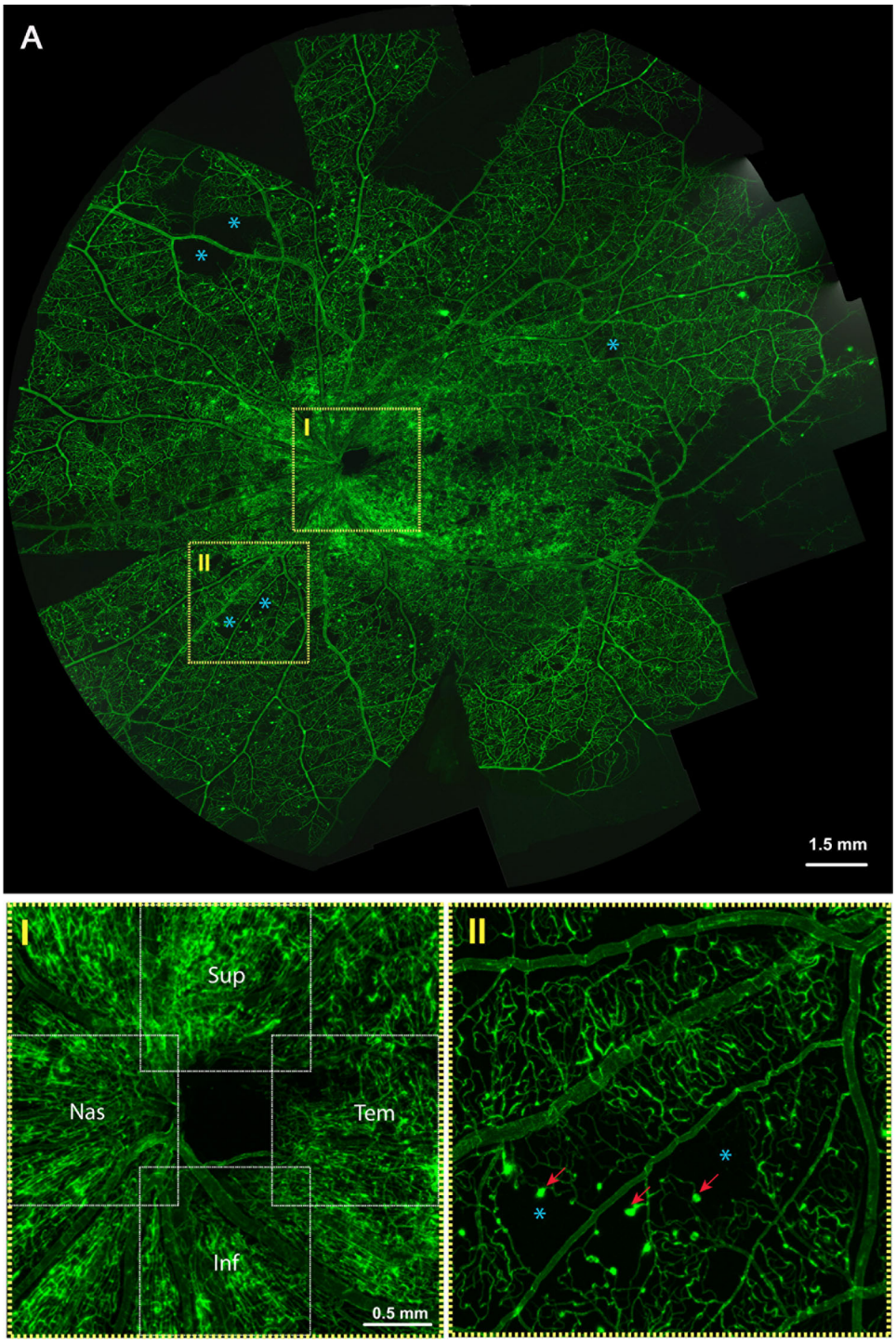

Figure 1. Representative whole-mount microscopy image of a donor eye in the diabetes group following perfusion-based vascular labeling. The low-magnification montage (**A**) reveals multiple areas of nonperfusion (stars). High-magnification image of the peripapillary region (I) demonstrates clear delineation of capillary structures but note that there is increased staining and some leakage of vascular structures. Inset of a site distal to the peripapillary region (II) highlights the histologic features of nonproliferative diabetic retinopathy such as microaneurysms (arrows) and capillary nonperfusion (star). The peripapillary region in the diabetes group was divided into superior (Sup), temporal (Tem), inferior (Inf), and nasal regions (Nas) for quantitative analysis.

Capillary density was observably reduced in the DCP in four of seven eyes in the diabetes group (Figs. 3, 4). Visualization of confocal volumes at different angles of rotation (Fig. 5) allowed precise identification of capillary segments in the DCP with reduced or a total absence of endothelial stain. A spectrum of vascular alterations was seen in the DCP in the diabetes group ranging from focal disruptions of single capillary segments within a capillary loop to profound disorganization of the entire plexus (Fig. 4). In some eyes, it was not possible to clearly discern the closed-loop morphol-

Investigative Ophthalmology & Visual Science

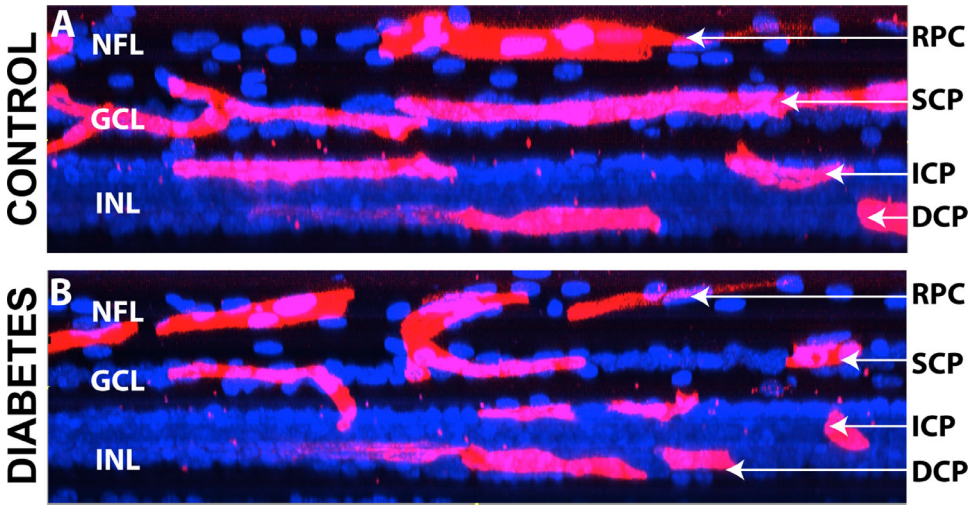

Figure 2. Spatial organization of peripapillary capillary plexuses. Transverse histologic sections with endothelial staining (purple) co-localized to nuclei (blue) demonstrates that the peripapillary region of the control (**A**) and diabetes (**B**) groups is comprised of four capillary plexuses: the RPC plexus at the level of the NFL, SCP at the level of the ganglion cell layer (GCL), the ICP at the inner border of the inner nuclear layer (INL), and the DCP at the boundary of the INL and outer plexiform layer.

ogy of the DCP due to the extensive loss of capillary structures (Fig. 4D).

We did not find any cases where there was an observable reduction in capillary density in the RPCP, SCP, or ICP alone, whereas the DCP seemed morphologically normal. Microaneurysms were seen in two of seven eyes (donor 1L, 5R) in the peripapillary area of the diabetes group. There were 0% of microaneurysms that were localized to the RPCP, 6% to the SCP, 30% to the ICP, and 64% to the DCP (Fig. 4). No intraretinal edema/cysts were identified in any of the diabetic retinas within the peripapillary region.

Quantitative Analysis of the Diabetes Group

Measurements of capillary diameter and capillary density for the diabetes group are provided in Tables 2 and 3, respectively. Capillary diameter did not differ between any plexus (all $P > 0.050$). The RPCP, SCP, and ICP had comparable mean intercapillary distances (all $P > 0.050$) and they were all significantly denser than the DCP (all $P < 0.001$).

There was no significant difference among the superior, inferior, nasal, and temporal quadrants for capillary diameter and density measurements in the diabetes group (all $P > 0.050$).

Quantitative Comparisons of Capillary Diameter and Density Measurements Between the Control and Diabetes Groups

Age, sex, and time to cannulation were not significantly associated with capillary diameter and density for both diabetes and control groups (all $P > 0.050$). Mean capillary diameter measurements for each plexus of the control and diabetes groups are provided in Table 2 ($n = 9360$). Mean capillary diameter of all the plexuses was significantly higher in the diabetes group (9.1 ± 1.2 µm; $n = 5040$) compared to the control group (6.6 ± 0.9 µm; $n = 4320$; $P < 0.001$). Comparisons of individual capillary plexuses revealed that capillary diameter was significantly increased in the SCP only in the diabetes group ($P = 0.004$). Capillary diameter in the diabetes group was significantly greater in the nasal, temporal, superior, and inferior quadrants compared to the control group (all $P < 0.050$).

Mean capillary density measurements for each plexus of the control and diabetes groups are provided in Table 3. Mean ICD of all the plexuses in the diabetes group (133.3 ± 82.8 µm) was significantly larger than the control group (99.5 ± 13.7 µm). Analysis of individual plexuses revealed significantly larger ICD in the diabetic RPCP (113.7 ± 52.6 µm vs. 89.4 ± 12.6 µm; $P = 0.022$) and DCP (178.1 ± 128.6 µm vs. 106.6 ± 8.3 µm; $P = 0.004$) compared to the control group. This difference was significant across all four quadrants of the peripapillary regions (all $P < 0.050$).

Quantitative Comparisons of Inflow and Outflow Pathways between the Control and Diabetes Groups

The patterns of inflow and outflow branching patterns in the diabetes group were the same as the control group. The frequencies of each branching pattern were, however, different in each group, as discussed below.

The frequencies of the different inflow branching patterns of the SCP in the control ($n = 51$) and diabetes ($n = 58$) groups are schematically illustrated in Figure 6. There was a statistically significant association between diabetes and capillary inflow pathways, chi-square(3) = 9.52; $P = 0.023$. The strength of the association was moderate,[37] Cramer's V = 0.296. Based on the analysis of residuals, patterns 1 and 2 were significant contributors, whereas patterns 3 and 4 were not significant contributors to the association.

The frequencies of the different branching patterns in the outflow pathway of the SCP in the control ($n = 51$) and diabetes ($n = 41$) groups are schematically illustrated in Figure 7. There was no significant association between diabetes and venous branching pattern, chi-square(3) = 1.13; $P = 0.771$.

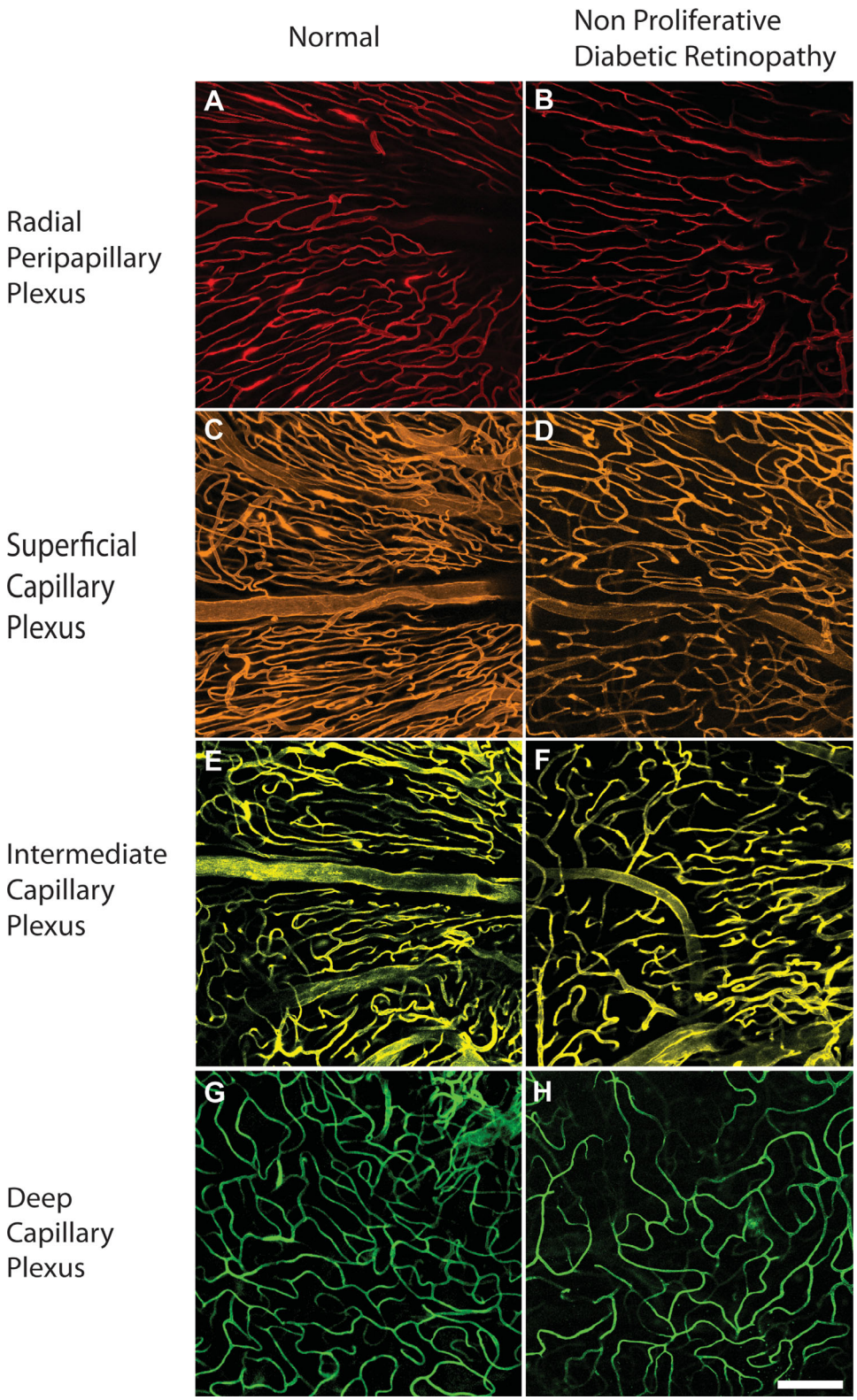

Figure 3. Comparisons of the morphologic characteristics of the peripapillary capillary plexuses between control eyes (donor 3L) and eyes with NPDR (donor 7L). En face projections of confocal images that composed the radial peripapillary capillary plexus (**A**, **B**), superficial capillary plexus (**C**, **D**), intermediate capillary plexus (**E**, **F**), and deep capillary plexus (**G**, **H**) are provided. Images in the *left* and *right* panels represent the control and diabetes groups, respectively. Note that the morphology of each capillary plexus in the control and diabetes groups is comparable. Mean capillary diameter is higher in the NPDR eye in the SCP (7.6 µm vs. 5.2 µm) and ICP (8.1 µm vs. 5.3 µm). Intercapillary distance is increased across all plexuses, with the largest difference at the RPCP (112.9 µm vs. 75.8 µm) and DCP (133.7 µm vs. 92.3 µm). Scale bar = 150 µm.

Investigative Ophthalmology & Visual Science

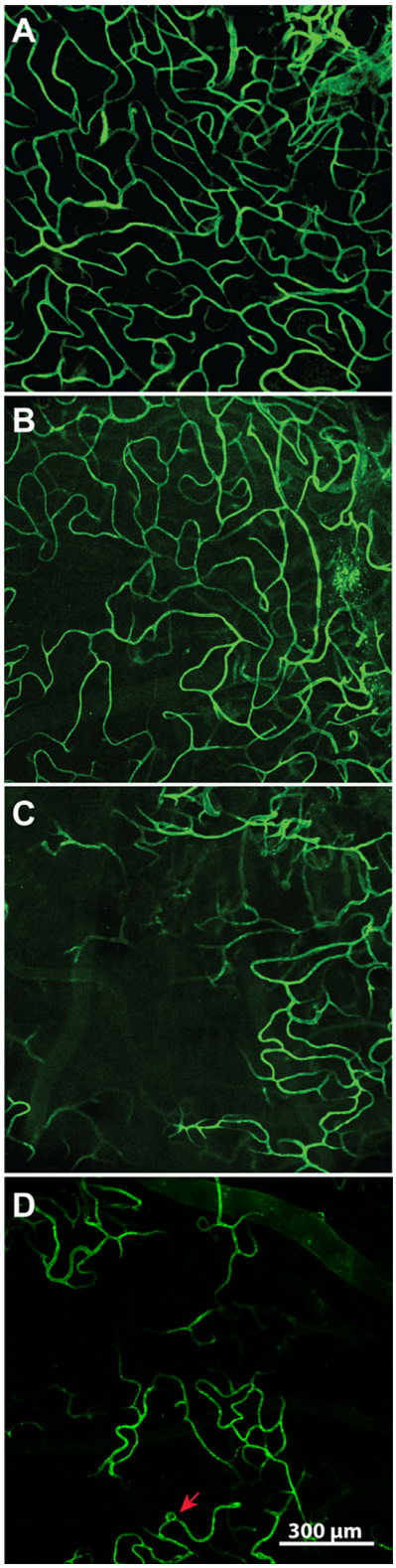

Figure 4. The spectrum of capillary density alteration in the DCP in the diabetes group. En face images of the DCP in four different donors in the diabetes group (**A**–**D**) reveal the range of DCP alterations, including focal disruptions of single capillary segments within a capillary loop to profound disorganization of the entire DCP. Arrow denotes a microaneurysm seen in the DCP.

Table 2. Capillary Diameter Measurements of Each Plexus in the Control and Diabetes Groups

	Control	Diabetes	*P* Value
All plexuses	6.6 ± 0.9 [4.3, 8.3]	9.1 ± 1. 2 [5.9, 12.1]	***<0.001***
RPCP	6.2 ± 1.1 [4.3, 8.3]	9.25 ± 1.34 [6.9, 11.2]	*0.088*
SCP	6.7 ± 0.8 [5.2, 7.9]	9.41 ± 1.03 [7.4, 11.3]	***0.004***
ICP	6.8 ± 0.81 [4.5, 8.1]	8.9 ± 1.02 [5.9, 10.6]	*0.085*
DCP	6.6 ± 0.8 [4.3, 7.7]	9.04 ± 1.20 [6.8, 12.1]	*0.182*

Mean ± standard error and range (µm) for each group is provided. Results of statistical comparisons between control and diabetes groups are provided in the right column.

Discussion

This study demonstrates that NPDR is characterized by disparate peripapillary capillary network alterations. We chose the peripapillary region as the area of interest as it can be reliably stratified into four capillary networks and because we have previously quantified the topologic properties of these networks in normal eyes.[32] The main findings of this study are as follows: (1) mean capillary diameter is increased in eyes with NPDR; (2) capillary density changes in NPDR are nonuniform with a predilection for the RPCP and DCP; and (3) alterations to capillary inflow pathways may precede capillary outflow pathway changes in NPDR.

The peripapillary microcirculation constitutes a highly complex network of capillary plexuses that are each morphologically different. In our previous study,[32] we demonstrated that the peripapillary circulation of the normal human eye can be stratified into four plexuses; the RPCP, SCP, ICP, and DCP. This is similar to the pig eye, as described by Rootman.[38] The works of our group[12,13,16] and others[39–41] have also shown that the microcirculations of other retinal eccentricities are similarly specialized. The reasons for the ramified organization of the retinal circulation are unclear but it is likely related to the unique physiologic and metabolic requirements of each retinal layer. For example, the RPCP resides at the level of the NFL and nourishes a predominantly axonal population, whereas the SCP, located at the level of the GCL, supports the energy demands of a large population of neuronal soma.[42] Other lines of evidence to demonstrate that the metabolic demands of the retina are heterogeneous include the significant variations in oxygen tension between retinal layers,[43] the nonuniform distribution of glial processes within the retina,[44,45] and the differences in neuroglobin[46] and cytochrome C oxidase[47] enzyme concentrations between retinal layers. Collectively, these findings suggest that certain retinal layers may be more, or less, vulnerable to injury following metabolic insults.

The role of microvascular alterations in the pathogenesis of DR is firmly established.[48] In his seminal work, Norman Ashton concluded that the three most important vascular manifestations that characterized DR include capillary closure, endothelial proliferation, and microaneurysms.[3] These findings were re-affirmed and expanded upon in the postmortem studies of other investigators.[1,49,50] In a significant number of histologic studies in the field of DR, trypsin digestion techniques were used for specimen preparation.[41] Although such methodology provided exquisite visualization of vascular detail, it resulted in the digestion of nonvascular components of the retina, making it difficult to precisely investigate microvascular changes relative to retinal depth. Using our perfusion-based endothelial labeling technique, coupled with nuclei labeling, we have been able

Investigative Ophthalmology & Visual Science

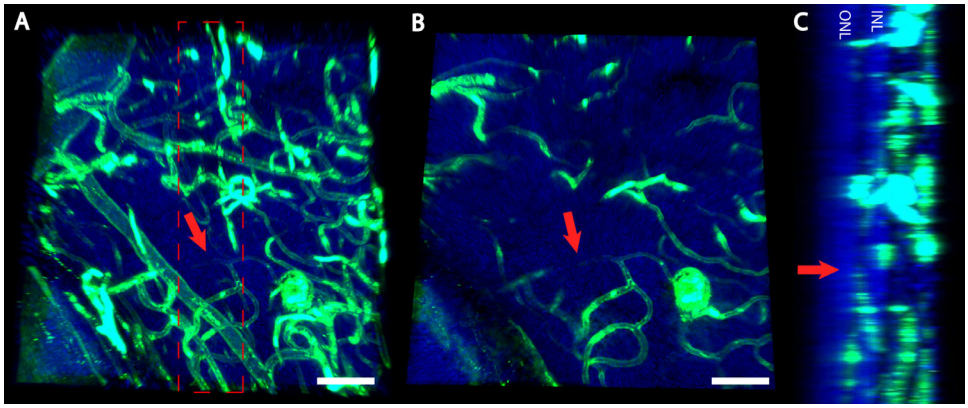

Figure 5. Selective nonperfusion of the DCP in the diabetes group. Visualization of the entire confocal volume (**A**) reveals numerous occluding vessels. One of these is marked with a red arrow. Visualization of the confocal volume from the same angle following removal of slices that depict the RPCP, SCP, and ICP (**B**) reveals that the site of attenuated vascular labeling is at the level of the DCP. Cross-sectional visualization of the area bound by *red box* in **A** shows intact retinal layers and that the vessel was occluded rather than displaced by intraretinal cyst or edema. ONL, outer nuclear layer; INL, inner nuclear layer. Scale bar = 90 µm.

Table 3. Intercapillary Distance Measurements of Each Plexus in the Control and Diabetes Groups

	Control	Diabetes	*P* Value
All plexuses	99.5 ± 13.7 [59.1, 130.3]	133.3 ± 82.8 [59.1, 564.4]	***<0.001***
RPCP	89.4 ± 12.6[59.1, 110.4]	113.7 ± 52.6 [59.1, 317.5]	***0.022***
SCP	96.8 ± 15.91 [70.6, 130.3]	115.0 ± 66.4 [68.6, 390.8]	*0.155*
ICP	105.5 ± 9.8 [87.6, 127.0]	126.5 ± 42.4 [79.4, 241.9]	*0.103*
DCP	106.6 ± 8.4 [92.4, 127.1]	178.1 ± 128.6 [94.1, 564.4]	***0.004***

Intercapillary distance was the metric used to determine capillary density hence plexuses of greater capillary density had relatively lower intercapillary distance measurements. Mean ± SE and range (µm) for each group is provided. Results of statistical comparisons between control and diabetes groups are provided in the right column.

to reliably stratify the capillary plexuses within the retina without tissue digestion.[16,51,52] Using this technique, capillaries that are denuded or manifest damaged endothelium are expected to show abnormal or absent lectin staining. This has allowed us to make reliable morphologic and quantitative comparisons between capillary plexuses and investigate the disparate pattern of vascular change in NPDR. In an OCTA study, Schreur et al. reported a high number of microaneurysms located in both the ICP and DCP, with the least number of microaneurysms found in the SCP. Our results slightly differ, as we found the highest percentage of microaneurysms in the DCP, followed by the ICP.

In this study, we show using lectin labeling that mean peripapillary luminal capillary diameter is increased by 2.5 µm in NPDR retina. Our findings are consistent with previous studies that have also revealed an increase in capillary diameter in eyes with diabetic retinopathy. In a human adaptive optics study of the macula, Burns et al. described an average capillary total diameter of 8.1 µm in 6 subjects with type 1 diabetes and 1 subject with type 2 diabetes, compared to an average capillary diameter of 6.1 µm in controls.[28] Similarly, Chui et al. found that a subject with proliferative DR had a capillary diameter of 7.7 to 10 µm across different regions of the macula, compared to 5.8 µm in a control subject.[29] In a Sprague-Dawley rat model, galactose fed diabetic rats had a retinal capillary diameter of 9.6 µm, which was significantly larger than 7.8 µm in control rats.[53] In contrast, Lombardo et al. reported a significant reduction in capillary lumen diameter in a group of 8 subjects with type 1 diabetes with mild NPDR.[54] One explanation for these differences may be the variation in the severity of diabetic retinopathy between studies. Taken together, these results may reflect a possible time sequence of pathological changes where thickening of the basement membrane[9,55,56] occurs first with associated narrowing of vessel lumen followed by enlargement of the lumen as a compensatory response as disease progresses.

In vivo adaptive optics scanning light ophthalmoscope fluorescein angiography[57] and OCTA[26] studies have shown a reduction in macular capillary density in eyes with diabetic retinopathy. Our present report is an extension of these previous important studies as it investigates whether there are uniform or nonuniform changes to the peripapillary retinal circulation in eyes with diabetic retinopathy. Specifically, we apply high-resolution confocal scanning laser microscopy to investigate the nature of capillary density changes within each plexus of the peripapillary region. Our findings implicate the DCP as the most vulnerable microcirculation to alteration in NPDR as it was the plexus with most significant reduction in density. Previous studies have provided evidence to suggest that the earliest manifestations of NPDR occur at the level of the deep retinal circulation. Simonett et al. and Carnevali et al. detected a significant reduction in perifoveal DCP density using OCTA, in patients with type 1 diabetes without DR or early DR.[58,59] Similar conclusion was drawn from patients with type 2 diabetes by Cao et al.[60] and Scarinici et al.[61] The reasons for the preferential vulnerability of the DCP to injury in DR are subject to conjecture but may relate to the greater oxygen demands of the OPL. Previous works done in macaque

Investigative Ophthalmology & Visual Science

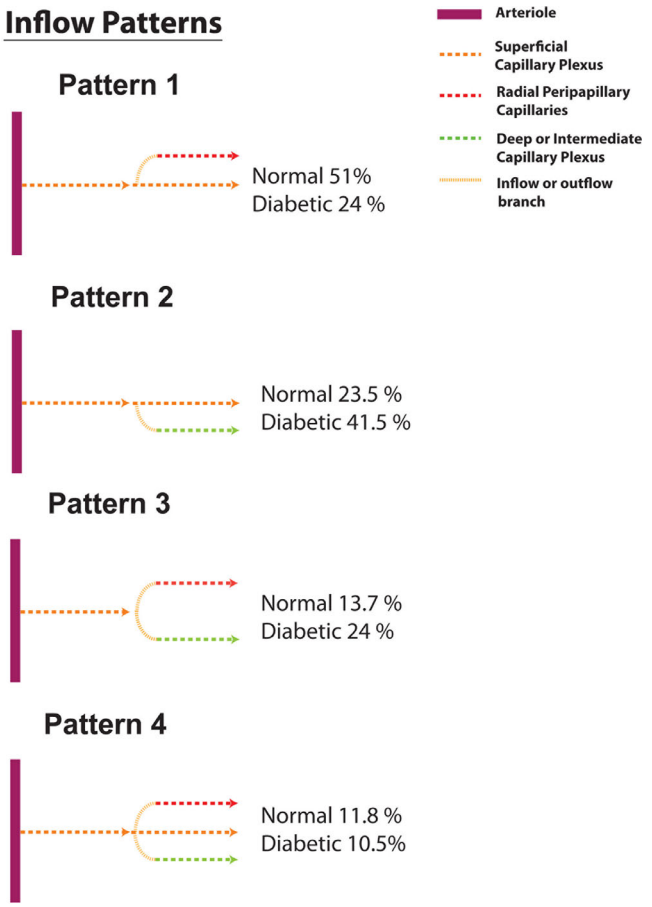

Figure 6. Patterns of capillary inflow of the SCP. Four different branching patterns were identified in the control and diabetes groups. The precapillary arteriole always connected to the SCP, after which connections to other capillary plexuses occurred. The frequencies of each of these patterns for each group are provided.

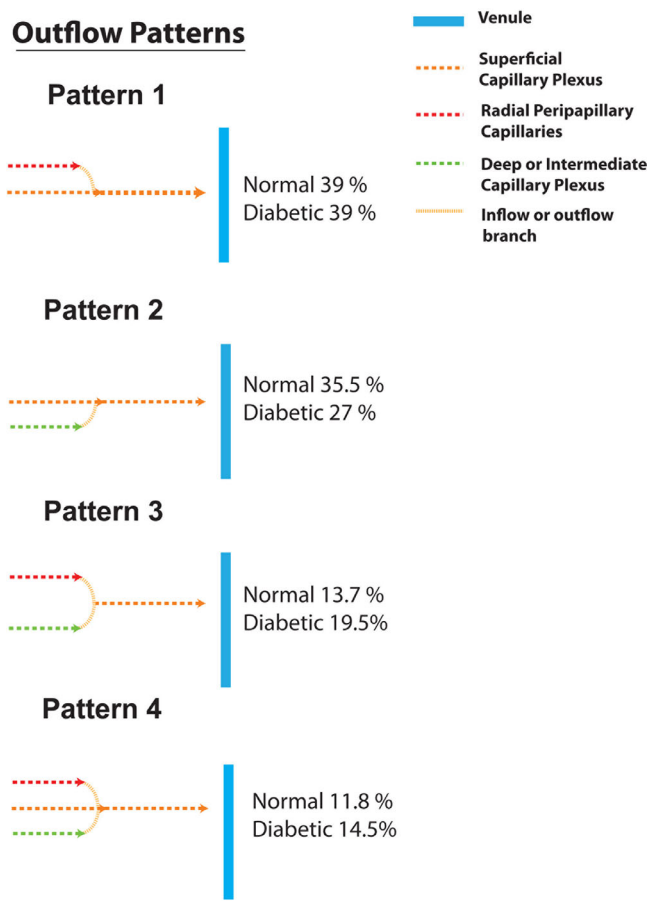

Figure 7. Patterns of capillary outflow of the SCP. Four different branching patterns were identified in the control and diabetes groups. Postcapillary venules only communicated with the SCP with no direct connections received from the radial peripapillary capillary plexus, SCP, or ICP. The frequencies of each of these patterns for each group are provided.

monkey retina by Ahmed et al. and rat retina by Yu and Cringle, utilizing oxygen sensitive microelectrodes to quantify intraretinal oxygen distribution, showed that oxygen consumption within the OPL was relatively greater than a number of other layers in the inner retina.[43,62] The greater oxygen consumption of the OPL may reflect the immense energy requirements of synaptic activity between rod and cone axons and the dendrites of bipolar and horizontal cells. Although we did not seek to investigate cause-effect relationships between structural changes in the OPL and DCP alterations, it is possible that disturbances in neurovascular coupling mechanisms in the OPL due to NPDR may underlie DCP changes.

The reduction in capillary density at the level of the DCP may underlie the significant change in capillary inflow pathways in eyes with NPDR. In this study, we found a greater frequency of inflow pathways connecting the SCP to the ICP/DCP in eyes with NPDR. This organization may reflect a compensatory response to localized ischemia and an attempt to increase blood flow to areas of reduced vascular density. Studies have shown that compensatory capillary modeling occurs in the brain following ischemic injury,[63,64] and in the retina following branch retinal vein occlusion.[65–67] We also found a lower frequency of pathways connecting the SCP to the RPCP in eyes with NPDR and this change may account for the reduction in RPCP density in DR. The preferential redirection of blood away from the RPCP may underlie the development of NFL thinning that is known to be an early feature of NPDR.[68] We did not identify any significant changes in the frequencies of capillary outflow pathways but this may be a manifestation of the more advanced stages of NPDR.

The results of this study may aid the clinical interpretation of OCTA data in the setting of DR. Recently, advances in OCTA software and hardware technologies have made it possible to resolve fine retinal vascular structures within the limits of 5 to 8 µm.[69] Quantifying and monitoring changes in capillary diameter and density in each of the retinal capillary plexuses using OCTA may, therefore, serve as a useful biomarker for detecting the onset of DR as well as monitoring disease progression. The application of volume-rendered OCTA techniques may also facilitate precise visualization of capillary inflow and outflow pathways and identify compensatory changes to blood flow patterns in response to regional ischemia. The strengths of this study include the excellent preservation of postmortem tissue in control and diabetes donor eyes as well as the perfusion-based endothelial labeling techniques applied to precisely study retinal capillary changes. In addition, confocal microscope has better rejection of scattered light, which allows precise imaging of the

Investigative Ophthalmology & Visual Science

diabetic retinal circulation in cases where intraretinal cysts and edema may cause displacement of capillary segments. However, we acknowledge several limitations of this study, namely the limited sample size of donor eyes as well as the lack of pre-mortem clinical information from diabetes donors to correlate with the histologic results. In addition, the number of microaneurysms identified using current perfusion labeling methodology may be underestimated, as only microaneurysms with patent lumens can be labeled. We also acknowledge that we have only investigated the peripapillary region in this report and it is possible that the spatial pattern, magnitude, and temporal sequences of capillary network alterations in other retinal eccentricities, such as the macula, may be different.

Acknowledgments

The authors thank the staff from the Lions Eye Bank of Western Australia, Lions Eye Institute, for provision of human donor eyes and staff from DonateLife WA, the Western Australian agency for organ and tissue donation who facilitated the recruitment of donors into the study by referral and completion of consent processes. We would also like to thank Vanessa K. Bowden, Research Fellow from the School of Psychological Science, The University of Western Australia, for her assistance with the statistical analyses.

Supported by the National Health and Medical Research Council of Australia.

Disclosure: **D. An,** None; **E. Chandrasekera,** None; **D.-Y. Yu,** None; **C. Balaratnasingam,** Novartis (C), Allergan (C), Bayer (C)

References

1. Cogan DG, Toussaint D, Kuwabara T. Retinal vascular pattern. IV Diabetic retinopathy. *Arch Ophthalmol*. 1961;66:366–378.
2. Flaxman SR, Bourne RRA, Resnikoff S, et al. Global causes of blindness and distance vision impairment 1990-2020: a systematic review and meta-analysis. *Lancet Glob Health*. 2017;5:e1221–e1234.
3. Ashton N. Studies of the retinal capillaries in relation to diabetic and other retinopathies. *Br J Ophthalmol*. 1963;47:521–538.
4. Ashton N. Pathophysiology of retinal cotton-wool spots. *Br Med Bull*. 1970;26:143–150.
5. Bek T. A clinicopathological study of venous loops and reduplications in diabetic retinopathy. *Acta Ophthalmol Scand*. 2002;80:69–75.
6. Bek T. Transretinal histopathological changes in capillary-free areas of diabetic retinopathy. *Acta Ophthalmol (Copenh)*. 1994;72:409–415.
7. Fryczkowski AW, Chambers RB, Craig EJ, Walker J, Davidorf FH. Scanning electron microscopic study of microaneurysms in the diabetic retina. *Ann Ophthalmol*. 1991;23:130–136.
8. de Oliveira F. Pericytes in diabetic retinopathy. *Br J Ophthalmol*. 1966;50:134–143.
9. Ashton N. Vascular basement membrane changes in diabetic retinopathy. Montgomery lecture, 1973. *Br J Ophthalmol*. 1974;58:344–366.
10. Aguilar E, Friedlander M, Gariano RF. Endothelial proliferation in diabetic retinal microaneurysms. *Arch Ophthalmol*. 2003;121:740–751.
11. Mizutani M, Kern TS, Lorenzi M. Accelerated death of retinal microvascular cells in human and experimental diabetic retinopathy. *J Clin Invest*. 1996;97:2883–2890.
12. Chan G, Balaratnasingam C, Yu PK, et al. Quantitative morphometry of perifoveal capillary networks in the human retina. *Invest Ophthalmol Vis Sci*. 2012;53:5502–5514.
13. Tan PE, Yu PK, Balaratnasingam C, et al. Quantitative confocal imaging of the retinal microvasculature in the human retina. *Invest Ophthalmol Vis Sci*. 2012;53:5728–5736.
14. Yu PK, Balaratnasingam C, Morgan WH, Cringle SJ, McAllister IL, Yu DY. The structural relationship between the microvasculature, neurons, and glia in the human retina. *Invest Ophthalmol Vis Sci*. 2010;51:447–458.
15. Yu DY, Yu PK, Cringle SJ, Kang MH, Su EN. Functional and morphological characteristics of the retinal and choroidal vasculature. *Prog Retin Eye Res*. 2014;40:53–93.
16. Yu PK, Mammo Z, Balaratnasingam C, Yu DY. Quantitative study of the macular microvasculature in human donor eyes. *Invest Ophthalmol Vis Sci*. 2018;59:108–116.
17. Dimitrova G, Chihara E. Implication of deep-vascular-layer alteration detected by optical coherence tomography angiography for the pathogenesis of diabetic retinopathy. *Ophthalmologica*. 2019;241:179–182.
18. Forte R, Haulani H, Jurgens I. Quantitative and qualitative analysis of the three capillary plexuses and choriocapillaris in patients with type 1 and type 2 diabetes mellitus without clinical signs of diabetic retinopathy: a prospective pilot study [published online ahead of print October 23, 2018. *Retina*. https://doi.org/10.1097/IAE.0000000000002376.
19. Kaizu Y, Nakao S, Arima M, et al. Capillary dropout is dominant in deep capillary plexus in early diabetic retinopathy in optical coherence tomography angiography. *Acta Ophthalmol*. 2019;97:e811–e812.
20. Sambhav K, Abu-Amero KK, Chalam KV. Deep capillary macular perfusion indices obtained with OCT angiography correlate with degree of nonproliferative diabetic retinopathy. *Eur J Ophthalmol*. 2017;27:716–729.
21. Nesper PL, Roberts PK, Onishi AC, et al. Quantifying microvascular abnormalities with increasing severity of diabetic retinopathy using optical coherence tomography angiography. *Invest Ophthalmol Vis Sci*. 2017;58:BIO307–BIO315.
22. Mo S, Phillips E, Krawitz BD, et al. Visualization of radial peripapillary capillaries using optical coherence tomography angiography: the effect of image averaging. *PLoS One*. 2017;12:e0169385.
23. Bosch A, Scheppach JB, Harazny JM, et al. Retinal capillary and arteriolar changes in patients with chronic kidney disease. *Microvasc Res*. 2018;118:121–127.
24. Jumar A, Harazny JM, Ott C, et al. Retinal capillary rarefaction in patients with type 2 diabetes mellitus. *PLoS One*. 2016;11:e0162608.
25. Tan PE, Balaratnasingam C, Xu J, et al. Quantitative comparison of retinal capillary images derived by speckle variance optical coherence tomography with histology. *Invest Ophthalmol Vis Sci*. 2015;56:3989–3996.
26. Hwang TS, Jia Y, Gao SS, et al. Optical coherence tomography angiography features of diabetic retinopathy. *Retina*. 2015;35:2371–2376.
27. Kaizu Y, Nakao S, Yoshida S, et al. Optical coherence tomography angiography reveals spatial bias of macular capillary dropout in diabetic retinopathy. *Invest Ophthalmol Vis Sci*. 2017;58:4889–4897.
28. Burns SA, Elsner AE, Chui TY, et al. In vivo adaptive optics microvascular imaging in diabetic patients without clinically severe diabetic retinopathy. *Biomed Opt Express*. 2014;5:961–974.

29. Chui TY, Pinhas A, Gan A, et al. Longitudinal imaging of microvascular remodelling in proliferative diabetic retinopathy using adaptive optics scanning light ophthalmoscopy. *Ophthalmic Physiol Opt*. 2016;36:290–302.
30. Rabbani H, Allingham MJ, Mettu PS, Cousins SW, Farsiu S. Fully automatic segmentation of fluorescein leakage in subjects with diabetic macular edema. *Invest Ophthalmol Vis Sci*. 2015;56:1482–1492.
31. Arend O, Remky A, Harris A, Bertram B, Reim M, Wolf S. Macular microcirculation in cystoid maculopathy of diabetic patients. *Br J Ophthalmol*. 1995;79:628–632.
32. Chandrasekera E, An D, McAllister IL, Yu DY, Balaratnasingam C. Three-dimensional microscopy demonstrates series and parallel organization of human peripapillary capillary plexuses. *Invest Ophthalmol Vis Sci*. 2018;59:4327–4344.
33. Yu PK, McAllister IL, Morgan WH, Cringle SJ, Yu DY. Interrelationship of arterial supply to human retina, choroid, and optic nerve head using micro perfusion and labeling. *Invest Ophthalmol Vis Sci*. 2017;58:3565–3574.
34. Meyer W, Godynicki S, Tsukise A. Lectin histochemistry of the endothelium of blood vessels in the mammalian integument, with remarks on the endothelial glycocalyx and blood vessel system nomenclature. *Ann Anat*. 2008;190:264–276.
35. Agresti A. *Categorical data analysis*. 3rd ed. Hoboken, NJ: Wiley; 2013.
36. Wilkinson CP, Ferris FL, 3rd, Klein RE, et al. Proposed international clinical diabetic retinopathy and diabetic macular edema disease severity scales. *Ophthalmology*. 2003;110:1677–1682.
37. Cohen J. *Statistical power analysis for the behavioral sciences*. New York, NY: Psychology Press; 1998.
38. Rootman J. Vascular system of the optic nerve head and retina in the pig. *Br J Ophthalmol*. 1971;55:808–819.
39. Snodderly DM, Weinhaus RS, Choi JC. Neural-vascular relationships in central retina of macaque monkeys (*Macaca fascicularis)*. *J Neurosci*. 1992;12:1169–1193.
40. Snodderly DM, Weinhaus RS. Retinal vasculature of the fovea of the squirrel monkey, *Saimiri sciureus*: three-dimensional architecture, visual screening, and relationships to the neuronal layers. *J Comp Neurol*. 1990;297:145–163.
41. Kuwabara T, Cogan DG. Studies of retinal vascular patterns. Part 1. Normal architecture. *Arch Ophthalmol*. 1960;64:904–911.
42. Yu DY, Cringle SJ, Balaratnasingam C, Morgan WH, Yu PK, Su EN. Retinal ganglion cells: energetics, compartmentation, axonal transport, cytoskeletons and vulnerability. *Prog Retin Eye Res*. 2013;36:217–246.
43. Yu D-Y, Cringle SJ. Oxygen distribution and consumption within the retina in vascularised and avascular retinas and in animal models of retinal disease. *Prog Retina Eye Res*. 2001;20:175–208.
44. Distler C, Weigel H, Hoffmann KP. Glia cells of the monkey retina-I. Astrocytes. *J Comp Neurol*. 1993;333:134–147.
45. Distler C, Dreher Z. Glia cells of the monkey retina-II. Muller cells. *Vision Res*. 1996;36:2381–2394.
46. Ostojic J, Grozdanic SD, Syed NA, et al. Patterns of distribution of oxygen-binding globins, neuroglobins and cytoglobin in human retina. *Arch Ophthalmol*. 2008;126:1530–1536.
47. Yu DY, Cringle SJ, Yu PK, Su EN. Intraretinal oxygen distribution and consumption during retinal artery occlusion and graded hyperoxic ventilation in the rat. *Invest Ophthalmol Vis Sci*. 2007;48:2290–2296.
48. Lechner J, O'Leary OE, Stitt AW. The pathology associated with diabetic retinopathy. *Vision Res*. 2017;139:7–14.
49. Garner A. Histopathology of diabetic retinopathy in man. *Eye (Lond)*. 1993;7(Pt 2):250–253.
50. de VG, Davis M, Engerman R. Clinicopathologic correlations in diabetic retinopathy. I. Histology and fluorescein angiography of microaneurysms. *Arch Ophthalmol*. 1976;94:1766–1773.
51. Balaratnasingam C, An D, Sakurada Y, et al. Comparisons between histology and optical coherence tomography angiography of the periarterial capillary-free zone. *Am J Ophthalmol*. 2018;189:55–64.
52. An D, Balaratnasingam C, Heisler M, et al. Quantitative comparisons between optical coherence tomography angiography and matched histology in the human eye. *Exp Eye Res*. 2018;170:13–19.
53. Robison WG, Laver NM, Jacot JL, Glover JP. Sorbinil prevention of diabetic-like retinopathy in the galactose-fed rat model. *Invest Ophthalmol Vis Sci*. 1995;36:2368–2380.
54. Lombardo M, Parravano M, Serrao S, Ducoli P, Stirpe M, Lombardo G. Analysis of retinal capillaries in patients with type 1 diabetes and nonproliferative diabetic retinopathy using adaptive optics imaging. *Retina*. 2013;33:1630–1639.
55. Tsilibary EC. Microvascular basement membranes in diabetes mellitus. *J Pathol*. 2003;200:537–546.
56. Abrahamson DR. Recent studies on the structure and pathology of basement membranes. *J Pathol*. 1986;149:257–278.
57. Pinhas A, Razeen M, Dubow M, et al. Assessment of perfused foveal microvascular density and identification of nonperfused capillaries in healthy and vasculopathic eyes. *Invest Ophthalmol Vis Sci*. 2014;55:8056–8066.
58. Simonett JM, Scarinci F, Picconi F, et al. Early microvascular retinal changes in optical coherence tomography angiography in patients with type 1 diabetes mellitus. *Acta Ophthalmol*. 2017;95:e751–e755.
59. Carnevali A, Sacconi R, Corbelli E, et al. Optical coherence tomography angiography analysis of retinal vascular plexuses and choriocapillaris in patients with type 1 diabetes without diabetic retinopathy. *Acta Diabetol*. 2017;54:695–702.
60. Cao D, Yang D, Huang Z, et al. Optical coherence tomography angiography discerns preclinical diabetic retinopathy in eyes of patients with type 2 diabetes without clinical diabetic retinopathy. *Acta Diabetol*. 2018;55:469–477.
61. Scarinci F, Nesper PL, Fawzi AA. Deep retinal capillary nonperfusion is associated with photoreceptor disruption in diabetic macular ischemia. *Am J Ophthalmol*. 2016;168:129–138.
62. Ahmed J, Braun RD, Dunn R, Jr, Linsenmeier RA. Oxygen distribution in the macaque retina. *Invest Ophthalmol Vis Sci*. 1993;34:516–521.
63. Ostergaard L, Jespersen SN, Mouridsen K, et al. The role of the cerebral capillaries in acute ischemic stroke: the extended penumbra model. *J Cereb Blood Flow Metab*. 2013;33:635–648.
64. Guo H, Itoh Y, Toriumi H, et al. Capillary remodeling and collateral growth without angiogenesis after unilateral common carotid artery occlusion in mice. *Microcirculation*. 2011;18:221–227.
65. Tsuboi K, Sasajima H, Kamei M. Collateral vessels in branch retinal vein occlusion: anatomic and functional analyses by OCT angiography. *Ophthalmol Retina*. 2019;3:767–776.
66. Suzuki N, Hirano Y, Tomiyasu T, et al. Collateral vessels on optical coherence tomography angiography in eyes with branch retinal vein occlusion. *Br J Ophthalmol*. 2019;103:1373–1379.

Investigative Ophthalmology & Visual Science

67. Kokolaki AE, Georgalas I, Koutsandrea C, Kotsolis A, Niskopoulou M, Ladas I. Comparative analysis of the development of collateral vessels in macular edema due to branch retinal vein occlusion following grid laser or ranibizumab treatment. *Clin Ophthalmol*. 2015;9:1519–1522.
68. Carpineto P, Toto L, Aloia R, et al. Neuroretinal alterations in the early stages of diabetic retinopathy in patients with type 2 diabetes mellitus. *Eye (Lond)*. 2016;30:673–679.
69. Kashani AH, Chen CL, Gahm JK, et al. Optical coherence tomography angiography: a comprehensive review of current methods and clinical applications. *Prog Retin Eye Res*. 2017;60:66–100.

Investigative Ophthalmology & Visual Science